J. Webster (ed.), *Wiley Encyclopedia of Electrical and Electronics Engineering*
Copyright © 1999 John Wiley & Sons, Inc.

MICROWAVE SOLID STATE DEVICES

Microwave and millimeter wave solid-state devices are used in applications in the 3 GHz to 300 GHz frequency range. These devices can be divided into two large groups: two-terminal devices, or diodes, and three-terminal devices, or transistors. Diodes can be subdivided into passive and active devices, which refers to whether the real part of the impedance is positive or negative, respectively. Active diodes can further be classified according to the origin of the negative resistance. The three-terminal active devices are divided into minority and majority carrier devices. The classification is summarized as follows:

(1) Two-terminal devices
   a. Passive diodes
      - Schottky barrier diode
      - PIN diode
   b. Active diodes
   a. Transit-time effect based on
      - Avalanche injection: IMPATT diode, TRAPATT diode
      - Forward injection: BARITT diode
      - Tunnel injection: TUNNET diode
   b. Bulk effect: Gunn diode
   c. Tunnel effect: tunnel diode

(2) Three-terminal devices
   a. Minority carrier devices: BJT, *HBT*
   b. Majority carrier devices

- Field-effect transistor: *FET*, MOS, MESFET, *HEMT*

This article, focuses on the most frequently used microwave and millimeter wave devices: the Schottky barrier diode, PIN diode, IMPATT (impact avalanche transit time) diode, BARITT (barrier injection transit time) diode, Gunn diode, tunnel diode, MESFET (metal semiconductor field-effect transistor), *HEMT* (high-electron mobility transistor), and *HBT* (heterojunction bipolar transistor). Nowadays, there is also an increasing interest in the use of MOS (metal–oxide–semiconductor) type transistors for applications in the 0.5 GHz to 2.5 GHz range. For each of these devices, we first explain briefly their physical operation. (A more detailed analysis of the device's solid-state physics can be found in the Reading List.) Next, we discuss the devices' properties and frequency limitations, and finally we outline their main applications.

Microwave and Millimeter Wave Diodes

Schottky Barrier Diode.

Description. The *p–n junction diode* (1) is discussed first, since this component serves as the foundation of many solid-state devices. A *p–n* junction is formed at the metallurgical interface of two regions in a semiconductor where one region contains impurity elements that create equivalent positive charges (*p*-type) and the other region contains impurities that create negative charges (*n*-type).

A Schottky barrier diode is formed by placing a metal layer directly onto a unipolar semiconductor substrate. When the metal and the semiconductor material are brought into contact, electrons in the material having higher Fermi energy diffuse into the material with lower Fermi energy. This process proceeds rapidly until the Fermi energies of the two materials are balanced. If the semiconductor is *n*-type (*p*-type) and the work function of the semiconductor is smaller (larger) than that of the metal, a potential barrier is formed at the metal–semiconductor boundary, exhibiting rectifying current-voltage characteristics. When reverse biased, the diode behaves as a voltage-dependent capacitance with low losses, because the reverse current is small. Diodes operated under this condition are called varactors.

Properties and Frequency Limitations. The small-signal equivalent circuit of the Schottky diode is shown in Fig. 1. It consists of an extrinsic and an intrinsic part. The extrinsic part consists of the parasitic elements that are inherent to the geometry of the device and hence depends on the way the device is inserted in the circuit. in Fig. 1, a Schottky diode in parallel configuration is shown. The parasitic capacitance C_{pg} and the inductance L_s are determined by the metallizations of the access lines to the device. The resistance R_s is the sum of the resistance of the anode metal and the ohmic cathode resistance. The intrinsic part is within the dashed rectangle. The resistance R_{gsf} models the current through the Schottky diode. The capacitance C_{gs} models the change in the depletion charge with respect to the voltage across the Schottky diode. R_{gs} models the charging resistance of the Schottky junction. The extrinsic elements are independent of the applied voltage, while the intrinsic elements are bias-dependent.

Important figures of merit are the cut-off frequency $f_c(V)$ and the dynamic cut-off frequency f_{cd}. For a given voltage V (typically 0 V) applied across the Schottky diode, the cut-off frequency $f_c(V)$ is defined as

$$f_c(V) = \frac{1}{2\pi R_s C_{gs}(V)} \qquad (1)$$

The dynamic cut-off frequency f_{cd}, defined for varactors, gives an indication of the nnear variation of the capacitance. It is defined as

$$f_{cd} = \frac{1}{2\pi R_s}\left(\frac{1}{C_{gs,min}} - \frac{1}{C_{gs,max}}\right) \qquad (2)$$

with R_s the series resistance and $C_{gs,min}$ and $C_{gs,max}$ the minimum and maximum capacitance values. The cut-off frequency $f_c(V)$ can be maximized by decreasing the series resistance and the capacitance. The ohmic cathode resistance is inversely proportional to the diode width, whereas the resistance of the anode metal is proportional to the width and inversely proportional to the square of the number of diode fingers (the layout of a diode consists typically of a number of anodes in parallel which are often called “fingers”). The capacitance is proportional to the width. This implies that there exists an optimal width to maximize the figures of merit.

Schottky diodes that must be compatible with a standard monolithic microwave integrated circuit (*MMIC*) technology are often realized by connecting the drain and source of a MESFET or *HEMT* device. Those Schottky diodes typically have cut-off frequencies up to a few hundred gigahertz. The f_c can be increased to

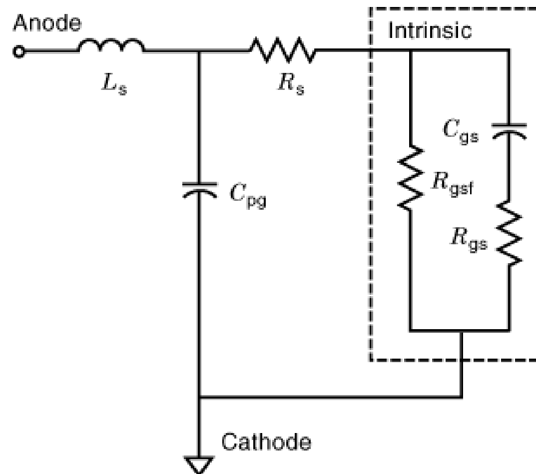

Fig. 1. Small-signal equivalent circuit of the Schottky diode in parallel configuration.

terahertz frequencies by modifying the layer structure and the layout (2). Schottky diodes for submillimeter wave applications are typically circular with an anode diameter of less than 2.5 μm.

Applications. Schottky diodes have been used extensively in nonlinear circuit applications during the past decades. At microwave and millimeter wave frequencies, Schottky diodes are now often replaced by transistors, because of their potential conversion gain. Schottky diodes are, however, still the basic nonlinear elements in microwave broadband mixers and in millimeter and submillimeter wave nonlinear applications. We can distinguish two modes of operation for Schottky diodes: the varistor and the varactor type.

In the first case, the diode is operated by utilizing the nonlinear characteristics in the forward-biased *I–V* curve. Varistors have potentially very large bandwidths. An important application is the mixer diode. This is a device that converts the input radio-frequency (RF) signal to a lower or higher frequency signal. As mentioned, the technology can be optimized for a certain application. In the case of mixer diodes, noise is an important specification. To reduce noise, the conversion loss should be decreased. This can be attained by a high carrier concentration and high-mobility material. From this point of view, gallium arsenide (GaAs), which has a higher mobility than silicon (Si), is currently used for high-sensitivity (low-noise) and high-frequency-operation mixer diodes. In addition to noise performance, the local oscillator drive level as a performance parameter of mixer diodes must be taken into account. Silicon is superior to GaAs from this point of view. The barrier height of the Schottky barrier contact on GaAs is fixed at 0.7 eV to 0.8 eV; therefore, a GaAs mixer diode usually requires a local oscillator drive level of 0 dBm to 10 dBm. On the other hand, a silicon mixer diode can be operated even at a local oscillator drive level of −10 dBm, because the barrier height can be varied by choosing the Schottky metal.

The second Schottky barrier diode type is the varactor. The term varactor comes from the words “variable reactor,” which means that the diode capacitance is variable with the external, reverse bias. Since the power consumption is theoretically zero, the potential power-added efficiency is high, but varactors exhibit a narrow fixed-tuned bandwidth. One application area of varactors is voltage-variable tuning. Such a varactor must possess high-capacitance change ratios, high values of the quality factor Q (defined as the ratio of energy stored to energy dissipated), and a wide voltage dynamic range. Since these values are related and generally involve trade-offs, elaborate design criteria should be established to determine the material and geometrical parameters of the diodes. A second application is harmonic generation, such as in frequency multipliers. By changing the layer structure, for example, by using hyper-abrupt junctions, the series resistance can be

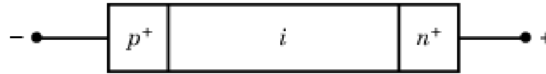

Fig. 2. Layer structure of the PIN diode.

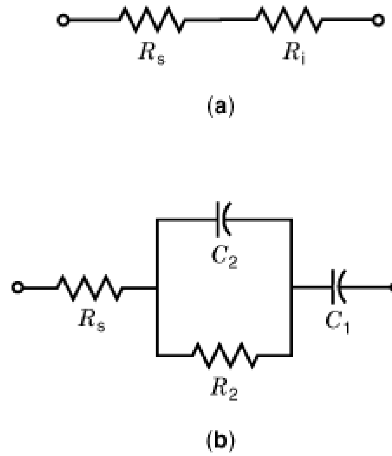

Fig. 3. Intrinsic small-signal equivalent circuit of the PIN diode in forward (a) and reverse (b) mode.

decreased and the characteristic of the capacitance as a function of the voltage can be optimized for particular designs. For example, for frequency triplers, a symmetrical profile around a dc bias of 0 V is preferred, since it suppresses the even order harmonics. This can be realized by means of a multiquantum well heterostructure varactor diode. Other varactor applications are nonlinear transmission lines, which require an abrupt $C(V)$ profile, *MMIC* phase shifters, and mixing detection.

PIN Diode.

Description. In a PIN diode, an intrinsic i layer is sandwiched between the p^+ and n^+ layers (Fig. 2). When the diode is forward biased, its impedance becomes low with the injection of carriers into the highly resistive intrinsic i layer, and the diode acts as a resistance. On the other hand, when the diode is reverse biased, the impedance becomes very high with spread of the depletion layer in the i layer, and the diode acts as a capacitance.

Properties and Frequency Limitations. The intrinsic small-signal equivalent circuit of the PIN diode at forward and reverse bias is shown in Fig. 3. As mentioned, this scheme needs to be completed by the appropriate extrinsic elements that strongly depend on the device configuration within the microwave or millimeter wave circuit and possible package. The resistance R_i is the i-layer resistance, R_s is the series resistance of the p^+ and n^+ layers, C_1 is the reverse-biased depleted capacitance, and C_2 and R_2 are the reverse-biased undepleted capacitance and resistance, respectively.

Important specifications of PIN diodes are low insertion loss, high power-handling capability, and fast switching time. In the ideal case, the lowest switching time is determined by the time to sweep away the stored charge in the i layer and is expressed by the transit time τ

$$\tau = \frac{V_\mathrm{b}}{E_\mathrm{max} v_\mathrm{s}} \tag{3}$$

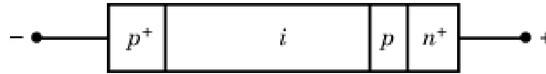

Fig. 4. Layer structure of the IMPATT diode.

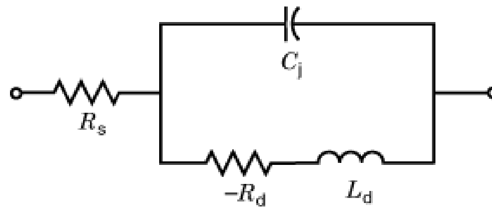

Fig. 5. Intrinsic small-signal equivalent circuit of the IMPATT diode.

where v_s is the saturation velocity of electrons, V_b is the breakdown voltage, and E_{max} is the electric field where breakdown occurs. Therefore, V_b must be low for faster switching. However, in actual diodes, the switching time is governed almost entirely by the parasitics of the diode.

For microwave applications, GaAs PIN diodes are often used instead of silicon because of the lower resistance of GaAs, reflecting higher mobility.

Applications. PIN diodes are used as phase shifters for phased-array radars, switches for pulsed radars, limiters to protect the receiver circuit against overload, and attenuators. In microwave integrated circuit (MIC) design, PIN diodes are preferred over Schottky diodes because their lower series resistance and capacitance leads to superior performance. The layer structure of PIN diodes is however not straightforwardly compatible with standard *MMIC* technology. Therefore, monolithic integrated phase shifter circuits are realized with Schottky diodes, cold field-effect transistors (*FET*s) (i.e., no dc current), or dual-gate *FET*s.

IMPATT Diode.

Description. The IMPATT (impact avalanche transit time) diode employs the impact ionization and transit properties of a semiconductor *p–n* junction to produce negative resistance at microwave frequencies. The diode type was first proposed by Read (3) in 1958. The p^+–i–p–n^+ layer structure is represented in Fig. 4. In operation the diode is reverse biased into avalanche breakdown. The *p* layer is the avalanche region, followed by a drift region, the *i* layer, for the generated charge carriers to drift. The electric field in this drift region should be high enough so that the generated carriers can travel at their saturation velocity.

When the diode is placed in a microwave resonant circuit, RF voltage fluctuations in the bias circuit increase and are forced into a narrow frequency range determined by the impedance characteristics of the resonant circuit. Because of the avalanche process, the RF current across the avalanche region lags the RF voltage by 90°. This inductive delay is by itself not sufficient to produce an active characteristic. However, when the 90° phase shift is added to that arising from an additional inductive delay caused by the transit time of the carriers drifting through the remainder of the diode external to the avalanche region, a phase shift between the RF voltage and current greater than 90° is obtained. A Fourier analysis of the resulting waveforms reveals a device impedance with a negative real part. That means that the device is active and can be used to generate or amplify RF signals. The device impedance has an S-type active characteristic, that is, its shape resembles the letter S.

Properties and Frequency Limitations. The intrinsic small-signal equivalent circuit of the IMPATT diode is shown in Fig. 5. It consists of the ohmic resistance R_s; the negative resistance R_d in series with the inductor L_d, which models the inductive delay; and the *p–n* junction capacitance C_j.

For optimum performance, the drift region is designed so that the electric field throughout the RF cycle is high enough to produce velocity saturation for the charge carriers. To achieve this, it is common to design

Fig. 6. Layer structure of the BARITT diode.

complex structures consisting of alternating layers of highly doped and lightly doped semiconductor regions. They can also be fabricated in a back-to-back arrangement to form double-drift structures. IMPATT diodes can be fabricated from most semiconductors but are generally fabricated from silicon or gallium arsenide.

Applications. IMPATT diodes are particularly attractive for millimeter wave applications and have been operated as high as a few hundred gigahertz. The devices are capable of good RF output power (mW to W) and good dc-to-RF conversion efficiency (approximately 10% to 20%). They have moderate bandwidth capability but relatively poor noise performance due to the impact ionization process.

BARITT Diode.

Description. Another diode belonging to the transit time diode family is the BARITT (barrier injection transit time) diode. The mechanisms responsible for the microwave oscillation are the thermoionic injection and diffusion of minority carriers across a forward-biased barrier and a transit time delay of the injected carriers traversing the drift region. Several structures can be operated as BARITT diodes, such as metal–n–metal, p–n–p, p–n–metal, etc.

The first BARITT operation was obtained from a metal–n–metal reach-through diode (4), shown in Fig. 6. It is basically two Schottky diodes connected back to back. When a sufficiently large bias is applied to the device, the electric field will reach through the entire device. Under this condition, thermoionic injection of holes across the barrier, located at the left metal-semiconductor interface, occurs. The injected holes traverse the drift region from this barrier to the right metal contact.

Properties and Frequency Limitations. The BARITT diode has no avalanche delay because the thermoionically injected carriers are in phase with the ac voltage swings. As a result, the efficiency of a BARITT diode is substantially lower than that of an IMPATT diode. This is because during a part of the period, both the ac voltage and current are positive. This implies that ac power is dissipated in the device. This power cancels some of the ac power generated by the device during the other part of the period. Therefore, the net ac power generated is smaller than the ac power of the IMPATT diode.

Applications. BARITT diodes are used in low-noise millimeter wave applications, since they are much less noisy than IMPATT diodes. The noise associated with carrier injection across the barrier is much less than the avalanche noise in an IMPATT diode. Disadvantages are the low efficiency and relatively narrow bandwidth.

Gunn Diode.

Description. The Gunn diode was developed by Gunn (5) in 1963. The name Gunn diode is given to all two-terminal devices whose operation depends on the transferred-electron effect. The Gunn diodes are a type of active diode. The negative conduction derives from the complex conduction band structure of certain compound semiconductor devices, such as GaAs and indium phosphide (InP). In these direct bandgap materials the central (or Γ) conduction band is in energy-momentum proximity to secondary, higher-order conduction bands (i.e., the X and L valleys). The electron effective mass is determined by the shape of the conduction bands. The electron effective mass is light in the Γ valley, but heavy in the higher-order X and L valleys. When the crystal is biased, the current flow is initially due to electrons in the light effective mass Γ valley, and hence the conduction is ohmic. However, as the bias field is increased, an increasing proportion of the free electrons are transferred into the X and L valleys, where the electrons have heavier effective mass. The increased effective mass slows down the electrons, with a corresponding decrease in conduction current through the crystal. The net result is that the crystal displays a region of applied bias voltages where current decreases with increasing

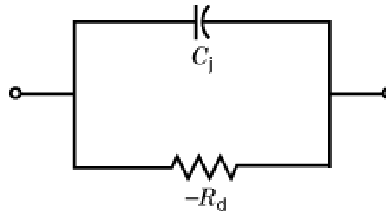

Fig. 7. Intrinsic small-signal equivalent circuit of the Gunn diode and the tunnel diode.

voltage, and a negative conductance is generated. The device is unstable and, when placed in an RF circuit or resonant cavity, oscillators or amplifiers can be realized. It is important to note that this device is not a diode in the strict sense, since no *p*–*n* or Schottky junction is used. The phenomenon is a characteristic of the bulk material and the special structure of the conduction bands in certain compound semiconductors. Most semiconductors do not have the conduction band structure necessary for the transferred electron effect.

Properties and Frequency Limitations. The intrinsic small-signal equivalent circuit of the Gunn diode is represented in Fig. 7. The Gunn diode can be modeled as a negative conductance $1/R_d$ in parallel with a capacitance C_j.

The bandwidth of the Gunn effect is limited by the speed with which the electrons can transfer from one valley to another and back. This is a scattering process which is characterized by a time constant. It turns out to be shorter in InP than in GaAs. In GaAs, the Gunn effect can be used to approximately 80 GHz, whereas in InP frequencies about twice as high can be reached.

Applications. Transferred electron devices are widely used in oscillators from the microwave through high millimeter wave frequency bands. They have good RF output power capability (milliwatts to watts level), moderate efficiency ($<$20%), and excellent noise and bandwidth capability. Octave band tunable oscillators are easily fabricated with YIG (yttrium iron garnet) resonators or varactors as the tuning element. Most commercially available solid-state sources for 60 GHz to 100 GHz operation generally use InP transferred electron devices. Compared with the IMPATT diode, the Gunn diode produces less output power but can exhibit lower noise performance.

Tunnel Diode.

Description. Tunnel diodes (6) generate active characteristics by a mechanism involving the physical tunneling of electrons between energy bands in highly doped semiconductors. For example, if a *p*–*n* junction diode is heavily doped, the conduction and valence bands are closely located and charge carriers can tunnel through the electrostatic barrier, separating the *p*-type and *n*-type regions, rather than be thermoionically emitted over the barriers as generally occurs in this type of diode. When the diode is (forward or reverse) biased, current immediately flows and the junction conduction is basically ohmic. In the forward bias direction, conduction occurs until the applied bias forces the conduction and valence bands to separate. The tunnel current then decreases and normal junction conduction occurs. In the forward bias region where the tunnel current is decreasing with increasing bias voltage, a negative immittance characteristic is generated. The immittance is called N-type because the *I*–*V* characteristic looks like the letter N.

Properties and Frequency Limitations. Tunnel diodes are described by a negative conductance $1/R_d$ in shunt with a capacitance C_j (Fig. 7). Tunnel diodes are limited in operation frequency by the time it takes for charge carriers to tunnel through the junction. Since this time is very short (on the order of 1 ps), the operation frequency can be very high, approaching 1 THz. They have been operated at hundreds of gigahertz, limited by practical packaging and parasitic impedance considerations. The RF power available from a tunnel diode is limited (hundreds of milliwatts level), because the maximum RF voltage swing that can be applied across the junction is limited by the forward turn-on characteristic of the device (typically 0.6 V to 0.9 V). Increased

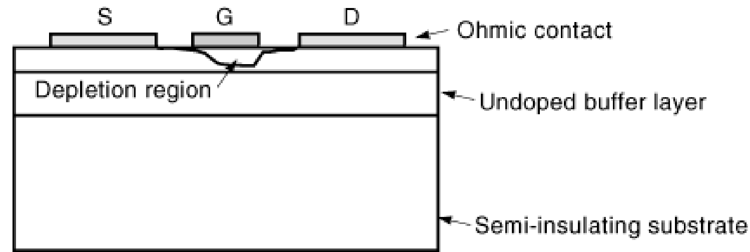

Fig. 8. Layer structure of the MESFET.

RF power can be obtained only by increasing device area to increase RF current, but device area is limited by operation frequency according to an inverse law.

Applications. Tunnel diodes have moderate dc–to–RF conversion efficiency (<10%) and very low noise figures and hence are useful in low-noise applications, such as microwave and millimeter wave receivers.

Microwave and Millimeter Wave Transistors

Field-Effect Transistor.

Description. The fundamental structure of the field-effect transistor (*FET*) has been proposed by Shockley in 1952 (7). An *FET* consists of an *n*-type semiconductor layer, sandwiched by *p*-type layers, and ohmic contacts, formed at the edges of the *n*-type layer. The ohmic contacts are called source and drain. The *p*–*n* junctions serve as a control element and are called the gate. When reverse bias is applied across the *p*–*n* junctions, space-charge regions form. Consequently, current flows from the drain to the source through a channel of the *n*-type layer bounded by the controlled space-charge regions.

Other types of *FET*s utilize different schemes for the gate from that of the *p*–*n* junction type. These types include the metal–insulator–semiconductor (MIS), in which a gate electrode is formed on the semiconductor via an insulator, and the metal–semiconductor (MES), in which a Schottky barrier is used as the gate. The most well known MIS transistor type is the metal–oxide–semiconductor *FET* (MOSFET) with an oxide as insulator. The cross section of the MESFET is represented in Fig. 8. Possible operation modes are the common-source configuration and the less frequently used common-gate configuration. In the former, the drain contact is biased at a specified potential (positive drain potential for an *n*-channel device) and the source is grounded. The flow of current through the conducting channel is controlled by negative dc and superimposed RF potentials applied to the gate, which modulate the channel current and provide RF gain. The current flow is composed of only one type of charge carrier (generally electrons) and the device hence is termed unipolar.

Properties and Frequency Limitations. The small-signal equivalent circuit and the definitions of the typical figures of merit are identical to those of *HEMT* devices and are therefore discussed in the corresponding part of the subsequent *HEMT* section.

Applications. There is an increasing interest in using several types of silicon MOSFETs (CMOS, SOI, LDMOS, etc.) in analog RF applications in the 0.5 GHz to 2.5 GHz frequency band (8, 9). For microwave applications, compound semiconductor materials, in particular gallium arsenide, are preferred. The reason is that GaAs electron mobility is six times as high and the peak drift velocity is twice as high as that of silicon. These properties result in larger transconductance, shorter electron transit times, and lower parasitic resistances. In addition, unlike silicon, semiinsulating GaAs substrates can be formed. This contributes to the simple structure of *FET*s and to an important reduction of parasitics. *p*–*n* junctions with fine patterns are difficult to realize in GaAs because of enhanced lateral diffusion at the surface. Metal-insulator-semiconductor

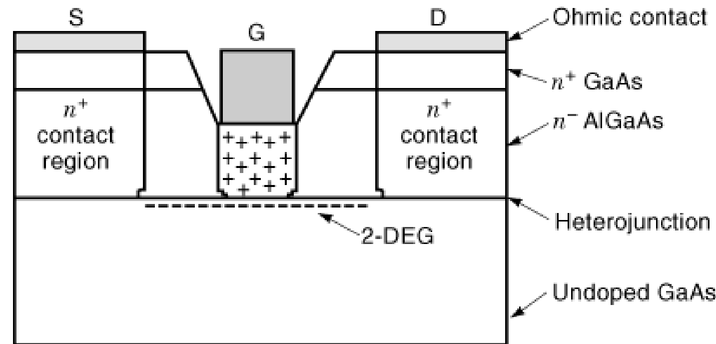

Fig. 9. Layer structure of the conventional AlGaAs–GaAs *HEMT*. 2-DEG, two-dimensional electron gas.

structures with a low interface state density, such as SiO_2–Si, are very difficult to obtain. On the other hand, GaAs MESFETs, fabricated for the first time by Mead in 1966 (10), have been widely successful. GaAs MESFETs are the most important active devices used in microwave applications, while the high-performant *HEMT*s are typically employed at millimeter wave frequencies. MESFETs can be optimized for small-signal, low-noise operation or for large-signal, RF power applications. Generally, low-noise operation requires short gate lengths, small gate widths, and highly doped channels. Power devices generally have longer gate lengths, much wider gate widths, and lower doped channels.

High-Electron Mobility Transistors.

Description. The high-electron mobility transistor (*HEMT*), first demonstrated by Dingle et al. in 1978 (11), owes its name to the high low-field mobility of its channel electrons, which are captured at the interface of two semiconductor materials with a different bandgap energy and with a similar lattice constant. This type of interface is called a heterojunction.

A schematic cross section of the conventional *HEMT*, based on the AlGaAs–GaAs heterojunction, is shown in Fig. 9. Free electrons provided by the n-doped AlGaAs layer diffuse across the heterojunction into the narrow bandgap GaAs and become captured in the quasi-triangular potential well at the interface caused by the conduction band discontinuity (ΔE_v). This leads to a two-dimensional electron gas consisting of electrons that are confined in the direction perpendicular to the heterojunction interface but free to move in parallel directions. Because of the spatial separation between carriers and dopants, electrons in the channel obtain a very high low-field mobility, especially at low temperatures. The flow of electrons between the source and ohmic drain contact regions is modulated using an external gate voltage applied on a Schottky gate contact. Although the bias on the Schottky gate contact controls the depth of the undepleted channel for a MESFET, for *HEMT*s the gate bias directly controls the carrier density in the channel.

The conventional lattice-matched AlGaAs–GaAs layer structure has now been widely replaced by other combinations of compounds, leading to improved *HEMT* characteristics. Conventional *HEMT* suffers from a small conduction band discontinuity ΔE_c; by incorporating indium in the channel, the conduction band discontinuity can be enhanced, leading to three additional types of *HEMT*s (indicated on the energy bandgap versus lattice constant diagram of Fig. 10):

(1) The pseudomorphic *HEMT* (P*HEMT*) grown on a GaAs substrate and based on the $Al_xGa_{1-x}As$–$In_yGa_{1-y}As$ heterojunction
(2) The InP lattice-matched *HEMT* (LM *HEMT*) grown on an InP substrate and based on the $Al_{0.48}In_{0.52}As$–$In_{0.53}Ga_{0.47}As$ heterojunction

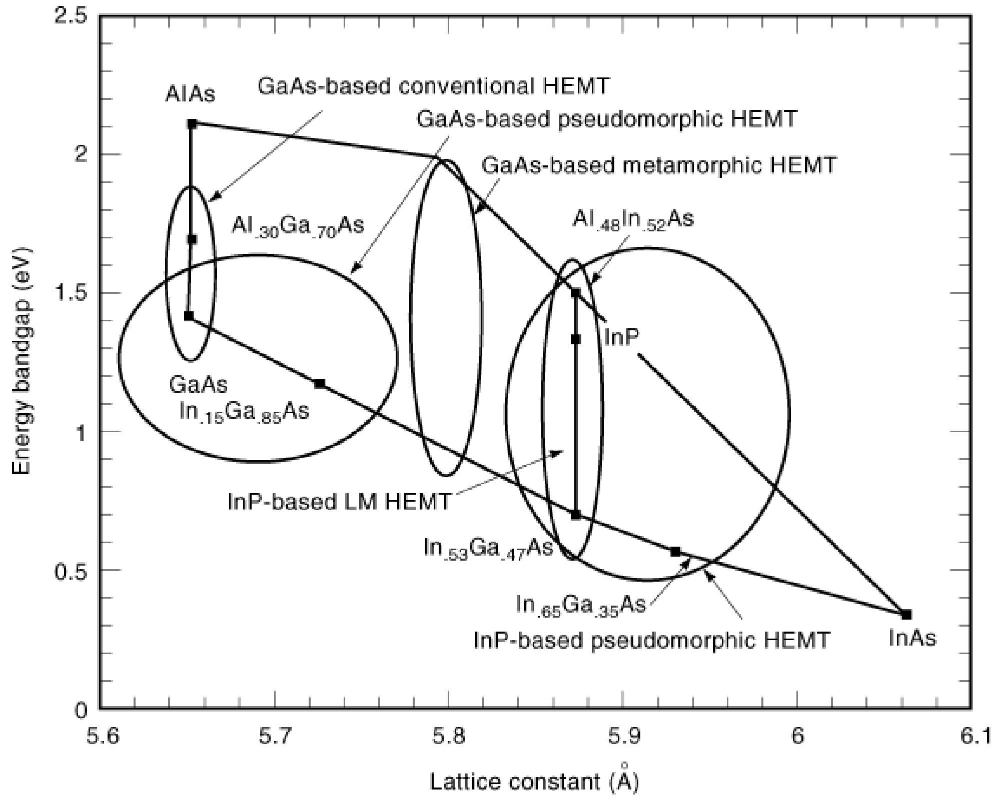

Fig. 10. Energy bandgap versus lattice constant diagram indicating the four different *HEMT* families.

(3) The InP pseudomorphic *HEMT* (InP P*HEMT*) grown on an InP substrate and based on the $Al_{0.48}In_{0.52}As$–$In_xGa_{1-x}As$ ($0.53 > x > 0.80$) heterojunction

For completeness, the relatively new GaAs-based metamorphic *HEMT* (MM *HEMT*) is also indicated in Fig. 10. This *HEMT* is grown strain-relaxed on GaAs and is based on the $Al_{1-y}In_yAs$–$In_xGa_{1-x}As$ ($0.3 < x < 0.5$) heterojunction (12).

Properties and Frequency Limitations. The small-signal equivalent circuit of the MESFET and *HEMT* devices is shown in Fig. 11. As has already been indicated above, the small-signal equivalent circuit consists of an extrinsic, bias-independent part and an intrinsic, bias-dependent part. The parasitic capacitances C_{pg}, C_{pd}, and C_{pgd} and the inductances L_s, L_d, and L_g are determined by the metallizations of the access lines to the device. It should be noted that in case of on-wafer devices, the measurements are typically deembedded up to the reference plane of the device, which is the device as it will be inserted in the actual circuit design. The effect of the probe pads hence is not included in this small-signal equivalent scheme. The resistances R_d and R_s are mainly caused by the drain and source ohmic contacts, and the gate resistance R_g is primarily determined by the gate Schottky contact. The intrinsic part is within the dashed rectangle. The resistances R_{gsf} and R_{gdf} model the current through the gate–source and gate–drain Schottky diodes. The capacitances C_{gs} and C_{gd} model the change in the depletion charge with respect to the gate–source V_{gs} and gate–drain V_{gd} voltages, respectively. The drain–source capacitance C_{ds} is included in the equivalent circuit to account for geometric capacitance effects between the source and the drain electrodes. The intrinsic gain mechanism of the

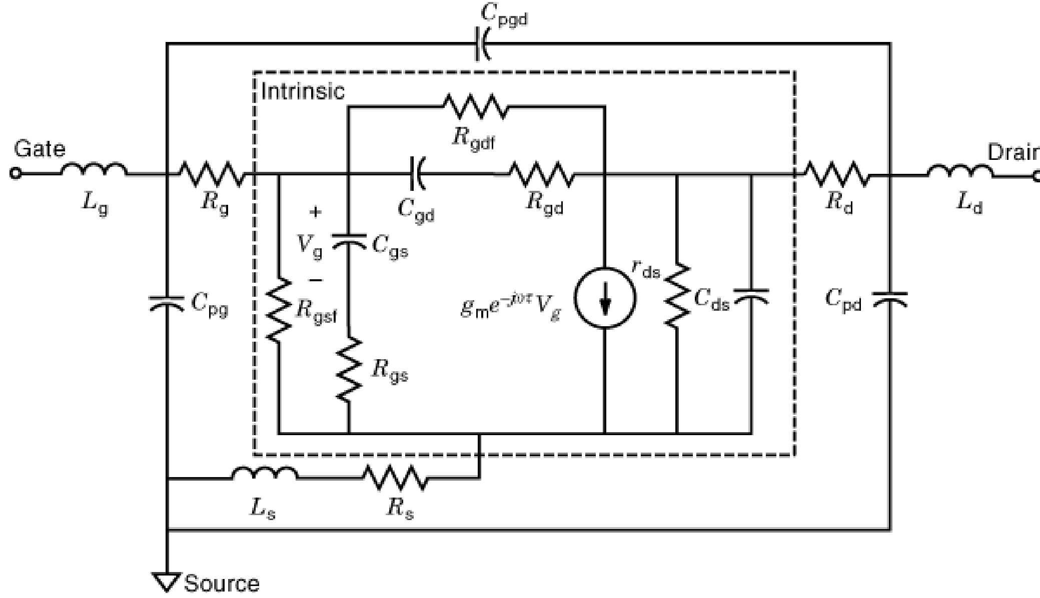

Fig. 11. Small-signal equivalent circuit of the MESFET and the *HEMT*.

HEMT is provided by the transconductance g_m, which is a measure of the incremental change in the drain–source output current I_{ds} for a given change in gate–source input voltage V_{gs}. Mathematically, it is defined as $g_m = \partial I_{ds}/\partial V_{gs}$. The output conductance g_{ds} is a measure of the incremental change in drain–source output current I_{ds} with the drain–source output voltage V_{ds}. It is defined mathematically as $g_{ds} = \partial I_{ds}/\partial V_{ds}$. R_{gs} and R_{gd} model the charging resistances in the channel. The transconductance cannot respond instantaneously to changes in the gate–source voltage V_{gs}. The delay inherent to this process is described by the transconductance delay τ. Physically, it represents the time it takes for the charge in the channel to redistribute itself after a fluctuation of V_{gs}.

Important figures of merit for MESFETs and *HEMT*s (13) are the transition frequency f_T and the maximum oscillation frequency f_{max}.

The transition or cut-off frequency f_T is defined as the frequency at which the short-circuit current gain (h_{21}) becomes unity. The h_{21} can be derived from the S-parameters as

$$h_{21} = \frac{-2S_{21}}{(1 - S_{11})(1 + S_{22}) + (S_{12}S_{21})} \tag{4}$$

To obtain a better physical understanding of the f_T, we express the intrinsic h_{21} in terms of the intrinsic small-signal elements

$$h_{21} = \frac{g_m}{2\pi(C_{gs} + C_{gd})f} \tag{5}$$

with f the frequency.

This equation indicates a −20 dB/decade roll-off for h_{21} and yields the usual approximate expression for the intrinsic f_T

$$f_{T,i} = \frac{g_m}{2\pi\,(C_{gs} + C_{gd})} \tag{6}$$

When the influence of the extrinsic resistances R_s and R_d (14) and the gate pad capacitance, defined as $C_{pad}=C_{pg} + C_{pgd}$, is taken into account, the expression for the transition frequency can be further refined to

$$\begin{aligned} f_T &= \frac{1}{2\pi\,\tau_T} \\ &= \frac{1}{2\pi}\left\{\frac{g_m}{(C_{gs} + C_{gd})}\left[1 + g_{ds}\,(R_s + R_d)\right] + C_{gd}\,g_m\,(R_s + R_d)\right. \\ &\quad \left. + \frac{g_{m,ext}}{C_{pad}}\right\} \end{aligned} \tag{7}$$

where $g_{m,ext}$ is the extrinsic transconductance and g_m represents the intrinsic transconductance.

The additional terms in this equation can be explained by a resistive divider effect at the output causing a current flow in the output resistance and thus reducing the short-circuit current with a factor $1 + g_{ds}(R_s + R_d)$, and by a Miller effect increasing the effective C_{gd} with a factor $1 + g_m(R_s + R_d)$. The influence of C_{pad} results in an extra charging time of the pad capacitance by the extrinsic transconductance $g_{m,ext}$.

For the derivation of the previous equations only the influence of the capacitances, resistances, and transconductance was taken into account leading to a −20 dB/decade roll-off for h_{21}. This fixed slope makes it possible to derive f_T by extrapolation from low-frequency measurements. When the influence of the inductances L_s and L_d is also taken into account, a h_{21} deviating from the −20 dB/decade slope is observed at high frequencies with a resonance behavior. Neglecting C_{gd}, the resonance frequency of the circuit can be approximated by

$$f_0 = \frac{1}{2\pi}\sqrt{\frac{1}{L_{in}C_{gs}} + \frac{1}{L_{in}C_{gs}}\left[1 - \frac{(R_{in}C_{gs} + g_m L_s)^2}{L_{in}C_{gs}}\right]} \tag{8}$$

with $L_{in}=L_g + L_s$ and $R_{in}=R_g + R_{gs} + R_s$. As a result of this behavior, the use of the original definition for f_T yields a cut-off frequency that is much higher than the extrapolated one. Still, as this artificially high f_T is not related with the physical device operation, the f_T value is generally determined by an extrapolation with a −20 dB/decade slope of the h_{21} measured at lower frequencies. Since the resonance behavior leads to a lower slope for h_{21} at high frequencies, and gate leakage can lead to a flattening and thus a lower slope of h_{21} at low frequencies, it is important not to rely on an extrapolation with an arbitrary slope, as is sometimes found in literature.

To obtain a high extrinsic f_T, it is necessary to have a small transit time of the electrons from the source to drain contact (15) and thus short gates, low access resistances R_s and R_d, a low output conductance g_{ds}, feedback capacitance C_{gd}, and pad capacitance C_{pad}.

The maximum oscillation frequency f_{max} is defined as the frequency for which the two-port becomes passive or the maximum power gain is unity. The derivation of f_{max} is more complicated than that of f_T, because there is no standard two-port parameter representing the maximum power gain. While the f_T can be derived directly from the short-circuit current gain h_{21}, the power gain is strongly dependent on the input and output matching networks.

In general, the transducer power gain G_T, which is the ratio of the power delivered to the load and the power available from the source, can be written as a function of the source and load reflection coefficients Γ_S and Γ_L

$$G_T = \frac{\left(1 - |\Gamma_S|^2\right) |S_{21}|^2 \left(1 - |\Gamma_L|^2\right)}{|(1 - S_{11}\Gamma_S)(1 - S_{22}\Gamma_L) - S_{12}S_{21}\Gamma_S\Gamma_L|} \qquad (9)$$

For an unconditionally stable two-port, the maximum transducer gain $G_{T,max}$ is obtained for a simultaneous conjugate match at both ports. For these conditions, $G_{T,max}$ is equal to the maximum available gain (*MAG*) (16) and is given by

$$G_{T,max} = \text{MAG} = \frac{|S_{21}|}{|S_{12}|}\left(K - \sqrt{K^2 - 1}\right) \qquad (10)$$

with K defined by Eq. (15).

The necessary and sufficient conditions for unconditional stability of a two-port network at a given frequency are (17, 18)

$$|\Gamma_S| < 1 \qquad (11)$$

$$|\Gamma_L| < 1 \qquad (12)$$

$$|\Gamma_{in}| = \left| S_{11} + \frac{S_{12}S_{21}\Gamma_L}{1 - S_{22}\Gamma_L} \right| < 1 \qquad (13)$$

$$|\Gamma_{out}| = \left| S_{22} + \frac{S_{12}S_{21}\Gamma_S}{1 - S_{11}\Gamma_S} \right| < 1 \qquad (14)$$

with Γ_{in} the input reflection coefficient and Γ_{out} the output reflection coefficient of the two-port network. These equations state that for all passive load impedances the real part of the input impedance must be positive and that for all passive source impedances the real part of the output impedance must be positive.

The following derived formula in (16) is often used. Unconditional stability requires that the two-port network meet the two inequalities

$$K = \frac{1 - |S_{11}|^2 - |S_{22}|^2 + |\Delta|^2}{2\,|S_{12}S_{21}|} > 1 \qquad (15)$$

and

$$|\Delta| = |S_{11}S_{22} - S_{12}S_{21}| < 1 \qquad (16)$$

For high-performance *HEMT*s, however, the relation $K < 1$ holds up to very high frequencies, such that in the normal measurement range the quantity *MAG* is not defined. For this range, in which the transistor

is potentially unstable, the maximum stable gain (*MSG*) can be used as a measure to calculate the potential gain of the device when inserted in an amplifier after being stabilized with a lossless network, for example, an inductive negative feedback network at the source, making $K = 1$

$$\mathrm{MSG} = \frac{|S_{21}|}{|S_{12}|} = \frac{g_{\mathrm{m,ext}}}{2}\pi f\left(C_{\mathrm{gd}} + C_{\mathrm{pgd}}\right) \qquad (17)$$

Unfortunately, the *MSG* and *MAG* have different slopes approximately −10 dB/decade and −20 dB/decade, respectively. This makes extrapolation with a fixed slope, as is done for the f_{T}, impossible. Therefore, the extrapolation of the $f_{\max}$ normally relies on the unilateral power gain U, or Mason's gain (19). This figure allows the derivation of an *MAG* for an unstable two-port as it is defined as the maximum available power gain when the two-port network is simultaneously conjugately matched while the feedback parameter Y_{12} is compensated for by an external lossless network. As shown by Rollett 20, this type of neutralization is possible for any two-port network. U is expressed by

$$U = \frac{1}{2}\frac{|S_{21}/S_{12} - 1|^2}{K\,|S_{21}/S_{12}| - \Re(S_{21}/S_{12})} = \frac{1}{4}\left(\frac{f_{\mathrm{T}}}{f}\right)^2 \frac{R_{\mathrm{ds}}}{R_{\mathrm{g}}} \qquad (18)$$

A second figure delivering an approximately −20 dB/decade slope over the whole region is the maximum unilateral transducer gain $G_{\mathrm{T}U,\max}$ which is the maximum available gain in the assumption that the device is unilateral ($S_{12} = 0$). For a unilateral device, the maximum gain is reached for $\Gamma_{\mathrm{S}} = S_{11}*$ and $\Gamma_{\mathrm{L}} = S_{22}*$, and is given by

$$G_{\mathrm{T}U,\max} = \frac{1}{1 - |S_{11}|^2}\,|S_{21}|^2\,\frac{1}{1 - |S_{22}|^2} \qquad (19)$$

The error made when S_{12} is set equal to zero can be estimated from the unilateral figure of merit F_U (16)

$$F_U = \frac{|S_{12}|\,|S_{21}|\,|S_{11}|\,|S_{22}|}{\left(1 - |S_{11}|^2\right)\left(1 - |S_{22}|^2\right)} \qquad (20)$$

The maximum error introduced by using $G_{\mathrm{T}U}$ instead of G_{T} is bounded by

$$\frac{1}{(1 + F_U)^2} < \frac{G_{\mathrm{T}}}{G_{\mathrm{T}U}} < \frac{1}{(1 - F_U)^2} \qquad (21)$$

Consistent with the theoretical derivation of the unilateral gain U, the modeled extrapolation to unity of both the $G_{\mathrm{T},\max}$ and U yield an identical $f_{\max}$. It should be noted that in practice the slopes of U, $G_{\mathrm{T}U,\max}$, and *MAG* deviate from their respective ideal slopes. Therefore, as usually only measurements at lower frequencies are available, the $f_{\max}$ is determined in practice using an extrapolation with a fixed −20 dB/decade slope.

An alternative way to determine $f_{\max}$ is to use the extracted small-signal model. However, as the analytical derivation of $f_{\max}$ is rather complicated, many approximate expressions for $f_{\max}$ can be found in literature, such

as (21)

$$f_{\max} = \frac{f_{\mathrm{T,i}}}{2\sqrt{g_{\mathrm{ds}}R_{\mathrm{in}} + \pi f_{\mathrm{T,i}}C_{\mathrm{gd}}\left(R_{\mathrm{in}} + R_{\mathrm{g}}\right)}} \tag{22}$$

whereby the influence of R_{gd}, C_{ds}, R_d, and of the transconductance delay have been neglected.

From this equation, it can be seen that to obtain a high f_{max}, it is important to have a high intrinsic f_T or a small transit time; a small gate resistance R_g, source resistance R_s, and channel charging resistance R_{gs}; a low output conductance g_{ds}; and a small parasitic C_{gd} associated with gate fringing.

Applications. High-electron mobility transistors are and will be employed in microwave and especially millimeter wave (wireless) telecommunication systems, automotive applications, and radioastronomy. Their main application is high-gain and low-noise amplifiers at frequencies ranging to beyond 100 GHz. According to the particular circuit specifications, the circuit designer selects the most appropriate *HEMT* technology (InP or GaAs based, lattice-matched, pseudomorphic, etc.)

An attractive configuration of the *HEMT* is the dual-gate *HEMT*. The dual-gate FET introduced in 1971 (22) is a MESFET with two parallel gate electrodes between drain and source. There are two main topologies for the dual-gate *HEMT*. In the first topology, an RF signal can be applied to the second gate. The second topology is the cascode configuration, which means that the second gate is RF grounded. This is equivalent with the cascade connection of a common-source *HEMT* and a common-gate *HEMT*. The RF input is the gate of the common-source *HEMT* and the RF output is the drain of the common-gate *HEMT*.

Figure 12 presents the (non)linear model of the dual-gate (cascode) *HEMT*. It consists of the cascade connection of the (non)linear models of two equivalent intrinsic single-gate *HEMT*s, supplemented with appropriate extrinsic elements (23). The parasitic elements consist of those of the equivalent single-gate *HEMT* and three additional elements: the feedback capacitance C_{pgd}, the substrate leakage resistance R_{sub} and the resistance between the two gates R_{int}. The capacitance C_{pg2} represents the extrinsic pad capacitance in case of the dual-gate device, and it represents the large capacitance to RF ground the second gate in case of the dual-gate cascode device. The requirement for this modeling approach is a uniform technology such that the physical characteristics, such as, V_T, of the single-gate *HEMT* for which the model is derived, are comparable to the characteristics of the dual-gate *HEMT*.

It is difficult to characterize the exact dc operating conditions of the dual-gate device, because the dc voltage controlling the second gate with respect to the floating point between the two gates and the dc voltage being applied to each part of the device is not externally measurable. This means that the normally used dc characteristics cannot give precise information on what really happens in the dual-gate *HEMT*. The representation of the bidimensional dc transfer characteristic (24) can be used to define the exact internal bias conditions and therefore the degree of saturation of each half of the dual-gate device. It is derived from the dc characteristics of the two single-gate devices that constitute the dual-gate device.

In the low frequency range, the dual-gate cascode *HEMT* can be represented by an equivalent single-gate *HEMT*. The main intrinsic elements (25) are given by

$$g_{\mathrm{m}} \approx g_{\mathrm{m1}}\frac{g_{\mathrm{m2}} + g_{\mathrm{ds2}}}{g_{\mathrm{m2}} + g_{\mathrm{ds2}} + g_{\mathrm{ds1}}} \tag{23}$$

$$g_{\mathrm{ds}} \approx g_{\mathrm{ds1}}\frac{g_{\mathrm{ds2}}}{g_{\mathrm{m2}} + g_{\mathrm{ds2}} + g_{\mathrm{ds1}}} \tag{24}$$

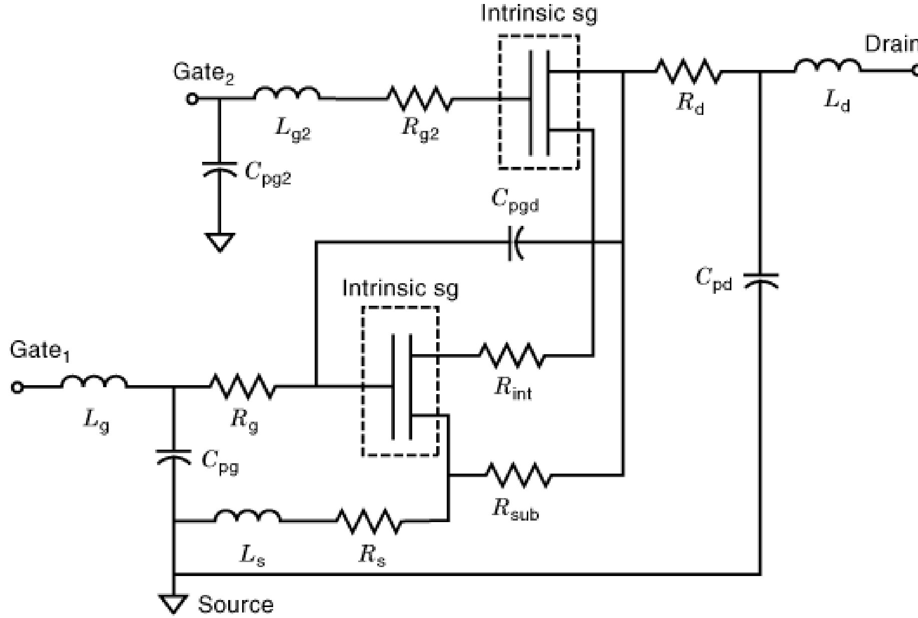

Fig. 12. Small-signal equivalent circuit of the dual-gate MESFET and *HEMT*.

$$C_{gs} \approx C_{gs1} + C_{gd1}\frac{g_{m2} + g_{ds1} + g_{m1}}{g_{m2} + g_{ds2} + g_{ds1}} \tag{25}$$

$$C_{gd} \approx C_{gd1}\frac{g_{ds2}}{g_{m2} + g_{ds2} + g_{ds1}} \tag{26}$$

where the indices 1 and 2 are for the common-source and common-gate transistor, respectively. In comparison with a single-gate *HEMT*, the transconductance g_m decreases slightly, the input capacitance C_{gs} increases, because of the Miller effect, and there is a significant reduction of the output conductance g_{ds} and the gate-drain capacitance C_{gd}. This implies that the cut-off frequency of the current gain f_T $(= g_m/2\,\pi\,C_{gs})$ is smaller and the *MSG* $\{\approx g_{m1}/\omega C_{gd1}\ [1 + g_{m2}/g_{ds2}]\}$ is theoretically higher than the figures of merit of the single-gate *HEMT*.

It is important to note that the dual-gate *HEMT* has suppressed kink and hence impact ionization (26), but the noise is slightly degraded compared with that of single-gate devices. The circuit applications for dual-gate (cascode) *HEMT*s are multiple (27). The dual-gate cascode configuration is applicable in several microwave circuits such as broadband distributed and variable gain amplifiers (28); active phase shifters (29); oscipliers (30), which combine self-oscillation and frequency multiplication; and self-oscillating mixers (31), which combine self-oscillation and mixing. The dual-gate *HEMT* is especially encountered in mixers (32) because of the inherent isolation between the local-oscillator signal and the RF signal.

Heterojunction Bipolar Transistors.

Description. The bipolar transistor (BJT) was invented by Bardeen and Brattain 33 in 1948. It consists of two back-to-back *p–n* junctions arranged in a sandwich structure. The three regions are designated the emitter, base, and collector. This type of device differs from *FET*s in that both electrons and holes are involved in the current transport process, which explains the term *bipolar*. Two structures are possible: *p–n–p* or *n–p–n*,

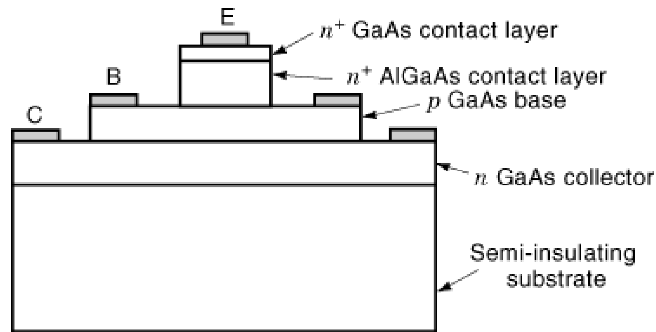

Fig. 13. Layer structure of the *HBT*.

depending upon the conductivity type common to both *p–n* junctions. For microwave applications the *n–p–n* structure is preferred, because device operation is controlled by electron flow. Electron transport is faster than that for holes, and hence *n–p–n* transistors are capable of superior high-frequency performance compared with comparable *p–n–p* transistors.

In operation, the base-emitter *p–n* junction is forward biased and the collector-base *p–n* junction is reverse biased. When an RF signal is applied to the base–emitter junction, the junction allows a current to be injected into the base region. The current in the base region consists of minority charge carriers, that is, carriers with the opposite polarity compared with the base material (e.g., electrons for an *n–p–n* transistor). These charge carriers then diffuse across the base region to the base–collector junction, where they are swept across the junction by the large reverse-bias electric field. The reverse-bias electric field in the base–collector region is generally made large enough that the carriers can travel at their saturation velocity. The transit time of the charge carriers across this region is small, except for millimeter wave transistors, where the base–collector region transit time can be a significant fraction of the total time required for a charge carrier to travel from the emitter through the collector.

The heterojunction bipolar transistor (*HBT*) is an improved high-frequency bipolar transistor that is fabricated using heterostructures of compound semiconductors. The emitter of this device is fabricated from a wide-bandgap semiconductor, and the remainder of the device is fabricated from a lower-bandgap semiconductor, for example, AlGaAs (emitter)/GaAs (base) (Fig. 13). This basic concept was proposed in 1957 by Kroemer 34. In an *n–p–n HBT*, the hole current flowing from base to emitter is suppressed by the potential barrier originating from the bandgap difference between the emitter and the base, which implies that a higher current injection efficiency is obtained compared with that of the homojunction bipolar transistor (35). This allows the base to be more heavily doped than the emitter, leading to a low base resistance and emitter–base capacitance, in contrast to the homojunction bipolar transistor, where the heavily doped base degrades the emitter injection efficiency. These three features—namely high emitter injection efficiency, low base resistance, and low emitter–base capacitance—are the essential points in obtaining high current gain at high frequencies.

The AlGaAs–GaAs heterojunction has been studied most intensively. Recently, the heterostructure concept has been applied in silicon-based devices using SiGe–Si heterostructures. The SiGe base has a lower bandgap than the germanium emitter, which allows the resistivity to be decreased with respect to homojunction bipolar transistors. Generally AlGaAs–GaAs *HBT*s exhibit superior performance to SiGe *HBT*s, but they require increased processing sophistication—that is, molecular beam epitaxy (MBE) versus standard epitaxial processing (36). The SiGe *HBT* technology has the great advantage of being compatible with standard silicon technology.

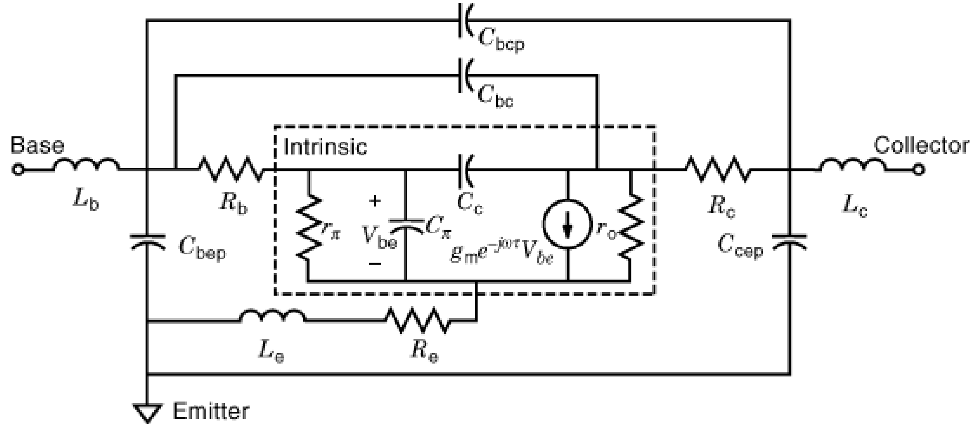

Fig. 14. Small-signal equivalent circuit of the *HBT*.

Properties and Frequency Limitations. The small-signal equivalent scheme of the *HBT* is presented in Fig. 14. This scheme consists also of a number of extrinsic, bias-independent and intrinsic, bias-dependent components. The parasitics associated with the access lines are represented by the shunt capacitances C_{bcp}, C_{bep}, and C_{cep}, and the series inductances L_{b}, L_{e}, and L_{c}. The distributed base–collector capacitance is modeled as a combination of the effective intrinsic capacitance C_{c} and the effective extrinsic capacitance C_{bc} (37). R_{e}, R_{b}, and R_{c} are the emitter, base, and collector series resistances, respectively. The intrinsic hybrid π network consists of the small-signal input resistance r_π, the collector output resistance r_{o}, the complex intrinsic transconductance g_{m} and the sum of the base–emitter depletion capacitance and the base charging capacitance, denoted by C_π.

The operation of the transistor is primarily controlled by the ability of the minority charge carriers to diffuse across the base region. For this reason, microwave transistors are designed with narrow base regions to minimize the time required for the carriers to travel through this region. The base region transit time is generally the limiting factor in determining the high-frequency capability of the transistor. The gain of the transistor is also significantly affected by minority carrier behavior in the base region. The density of minority carriers is significantly smaller than the density of majority carriers for typical operating conditions, and the probability that the minority charge will recombine with a majority carrier is high. If recombination occurs, the minority charge cannot reach the base–collector junction but appears as base current. This, in turn, reduces the current gain capability of the transistor. Narrow base regions reduce the semiconductor volume where recombination can occur and therefore result in increased gain. Typical base regions are on the order of 0.1 μm to 0.25 μm. The frequency response of a BJT can be determined by an analysis of the total time it takes for a charge carrier to travel from the emitter through the collector. The total time can be expressed as

$$\tau_{\text{ec}} = \tau_{\text{e}} + \tau_{\text{b}} + \tau_{\text{c}} + \tau_{\text{c}}' \tag{27}$$

where τ_{ec} is the total emitter–collector transit time, τ_{e} is the base–emitter junction capacitance charging time, τ_{b} is the base region transit time, τ_{c} is the base–collector junction capacitance charging time, and τ'_{c} is the base–collector region transit time. The total emitter–base time is related to the gain-bandwidth capability of the transistor according to the relation

$$f_{\text{T}} = \frac{1}{2\pi\,\tau_{\text{ec}}} \tag{28}$$

Since the BJT has three terminals, it can be operated in various configurations, depending on the electrode selected as the common terminal. The two most commonly employed are the common-emitter (*CE*) and the common-base (*CB*) configurations. The current gains of the transistor operated in the *CE* and *CB* configurations are called β and α, respectively. The *CE* current gain β is much larger than the *CB* current gain α, which is limited to values less than unity.

The static common-emitter current gain h_{FE}, which is the ratio of the collector current and the base current, is expressed by (38)

$$h_{\mathrm{FE}} = \frac{\alpha_0}{1-\alpha_0} \tag{29}$$

where α_0 is the dc current-gain with common-base configuration. The ac common-emitter current gain h_{fe} is expressed as

$$h_{\mathrm{fe}} = \frac{h_{\mathrm{FE}}}{1 + jh_{\mathrm{FE}}\omega/2\pi f_{\mathrm{T}}} \tag{30}$$

Microwave power transistors are usually operated under a common-base configuration (39), since the power gain when operated under that configuration is higher than the gain obtained under a common-emitter configuration. A measure of the RF power gain for the transistor is indicated by the unilateral power gain U, which can be expressed as

$$U = \frac{\alpha_0}{16\pi^2 R_{\mathrm{b}} C_{\mathrm{c}} \left(\tau_{\mathrm{ec}} + \frac{R_{\mathrm{e}} C_{\mathrm{c}}}{\alpha_0}\right)} \tag{31}$$

The frequency at which U is reduced to unity, $f_{\max}$, is the maximum frequency at which the device will have active characteristics. This frequency (39) is

$$f_{\max} = \sqrt{\frac{f_{\mathrm{T}}}{8\pi R_{\mathrm{b}} C_{\mathrm{c}}}} \tag{32}$$

To maximize the high-frequency performance of a BJT, it is necessary to design the device so that it has high current gain f_{T}, low base resistance R_{b}, and low collector capacitance C_{c}. As R_{b} and C_{c} have an influence on f_{T}, optimization is needed.

Other important specifications for power transistors are the maximum available current density and the breakdown voltage.

Applications. Bipolar transistors operating to about 20 GHz are generally fabricated from silicon. They are useful in moderate gain, low-noise and low to high RF power applications. In the microwave frequency range, *HBT*s are employed in both low-noise and high RF power applications. Although BJTs and *HBT*s exhibit better phase-noise performance than *FET* devices, *FET*s generally have a better noise figure.

BIBLIOGRAPHY

1. W. Shockley, The theory of p–n junctions in semiconductors and p–n junction transistors, *Bell Syst. Tech. J.*, **28**: 435, 1949.
2. T. W. Crowe, et al. Progress toward solid-state local oscillators at 1 THz, *IEEE Microw. Guided Wave Lett.*, **6**: 207–208, 1996.

3. W. T. Read, A proposed high-frequency negative-resistance diode, *Bell Syst. Tech. J.*, **37**: 401–466, 1958.
4. D. J. Coleman S. M. Sze, A low-noise metal-semiconductor-metal (MSM) microwave oscillator, *Bell Syst. Tech. J.*, **50**: 1695, 1971.
5. J. B. Gunn, Microwave oscillation of current in III-V semiconductors, *Solid-State Commun.*, **1**: 88, 1963.
6. S. M. Sze, *Physics of Semiconductor Devices*, New York: Wiley-Interscience, 1981.
7. W. Shockley, A unipolar "field-effect" transistor, *Proc. IRE*, **40**: 1365–1376, 1952.
8. N. Camilleri, *et al.* Silicon MOSFETs, the microwave device technology for the 90s, *IEEE MTT-S Int. Microw. Symp. Digest*, Atlanta, GA, 1993, pp. 545–548.
9. G. Ma, *et al.* High efficiency LDMOS power *FET* for low voltage wireless communications, *IEEE IEDM Digest*, 1996, pp. 91–94.
10. C. A. Mead, Schottky barrier gate field-effect transistor, *Proc. IEEE*, **54**: 307–308, 1966.
11. R. Dingle, *et al.* Electron mobilities in modulation doped semiconductor heterojunction superlattices, *Appl. Phys. Lett.*, **33**: 665–667, 1978.
12. A. Cappy, Metamorphic InGaAs/AlInAs heterostructure field effect transistors: Layer growth, device processing and performance, *Proc. 8th Int. Conf. Indium Phosphide Rel. Mater. (IPRM)*, 1996, pp. 3–6.
13. L. Nguyen, L. Larson, U. Mishra, Ultra-high-speed modulation-doped field-effect transistors: A tutorial review, *Proc. IEEE*, **80**: 494–518, 1992.
14. P. J. Tasker, B. Hughes, Importance of source and drain resistance to the maximum fT of millimeter-wave MODFETs, *IEEE Electron. Device Lett.*, **10**: 291–293, 1989.
15. N. Moll, M. R. Hueschen, A. Fischer-Colbrie, Pulsed doped AlGaAs/InGaAs pseudomorphic MODFET's, *IEEE Trans. Electron Devices*, **35**: 878–886, 1988.
16. G. Gonzalez, *Microwave Transistors Amplifiers—Analysis and Design*, Englewood Cliffs, NJ: Prentice-Hall, 1984.
17. K. Kurokawa, Power waves and the scattering matrix, *IEEE Trans. Microw. Theory Tech.*, **13**: 194–202, 1965.
18. T. T. Ha, *Solid State Microwave Amplifier Design*, New York: Wiley-Interscience, 1981.
19. S. J. Mason, Power gain in feedback amplifiers, *IRE Trans. Circuit Theory*, **1**: 20–25, 1954.
20. J. M. Rollett, The measurement of the transistor unilateral gain, *IEEE Trans. Circuit Theory*, **12**: 91–97, 1965.
21. R. Soares, *GaAs MESFET Circuit Design*, Norwood, MA: Artech House, 1988.
22. J. A. Turner, *et al.* Dual-gate gallium-arsenide microwave field effect transistor, *Electron. Lett.*, **7**: 661–662, 1971.
23. D. Schreurs, *et al.* Non-linear table-based model for GaAs and InP dual-gate cascode *HEMT*s, *Proc. 4th Int. Workshop Integrated Nonlinear Microw. Millimeterwave Circuits (INMMC '96)*, 1996, pp. 83–88.
24. C. Tsironis, R. Meierer, Microwave wide-band model of GaAs dual-gate MESFETs, *IEEE Trans. Microw. Theory Tech.*, **30**: 243–251, 1982.
25. Y. K. Chen, *et al.* Comparisons of microwave performance between single-gate and dual-gate MODFET's, *IEEE Electron. Device Lett.*, **9**: 59–61, 1988.
26. W. Daumann, *et al.* InAlAs/InGaAs/InP HFET with suppressed impact ionization using dual-gate cascode-devices, *IEEE Electron. Device Lett.*, **17**: 488–490, 1996.
27. C. Tsironis, GaAs dual gate MESFET's and their applications in microwave circuits, *Acta Electronica*, **23**: 317–324, 1980.
28. Y. Baeyens, *et al.* Coplanar amplifiers up to W-band using InP dual-gate *HEMT*s, *Proc. Microw. and Optronics Conf. (MIOP '97)*, 1997, pp. 61–64.
29. S. K. Koul, B. Bhat, *Microwave and Millimeter Wave Phase Shifters Volume II: Semiconductor and Delay Line Phase Shifters*, Norwood, MA: Artech House, 1991.
30. A. S. Chu P. T. Chen, An osciplier up to K-band using dual-gate GaAs MESFET, *IEEE MTT-S Int. Microw. Symp. Digest*, 1980, pp. 383–386.
31. C. Tsironis, 12 GHz receiver with self-oscillating dual-gate mesfet mixer, *Electron. Lett.*, **17**: 617–618, 1981.
32. S. A. Maas, *Microwave Mixers*, 2nd ed., Norwood, MA: Artech House, 1993.
33. J. Bardeen, W. H. Brattain, The transistor, a semiconductor triode, *Phys. Rev.*, **74**: 230–231, 1948.
34. H. Kroemer, Theory of a wide-gap emitter for transistors, *Proc. IRE*, **45**: 1535–1537, 1957.
35. H. Kroemer, Heterostructure bipolar transistors and integrated circuits, *Proc. IEEE*, **70**: 13–25, 1982.
36. A. Chantre, *et al.* A highly manufacturable 0.35 μm SiGe *HBT* technology with 70 GHz $f_{\max}$, *Proc. 28th Eur. Solid-State Device Res. Conf.*, 1998, pp. 448–451.

37. M. B. Das, High-frequency performance limitations of millimeter-wave heterojunction bipolar transistors, *IEEE Trans. Electron Devices*, **35**: 604–614, 1988.
38. R. J. Chaffin, *Microwave Semiconductor Devices*, New York: Wiley, 1973.
39. R. Aliison, Silicon bipolar microwave power transistors, *IEEE Trans. Microw. Theory Tech.*, **27**: 415–422, 1979.

READING LIST

F. Ali, A. Gupta, *HEMTs and HBTs: Devices, Fabrication and Circuits*, Norwood, MA: Artech House, 1991.
R. Anholt, *Electrical and Thermal Characterization of MESFETs, HEMTs and HBTs*, Norwood, MA: Artech House, 1995.
M. T. Faber, J. Chramiec, M. E. Adamski, *Microwave and Millimeter-Wave Diode Frequency Multipliers*, Norwood, MA: Artech House, 1995.
M. J. Golio, *Microwave MESFETs and HEMTs*, Norwood, MA: Artech House, 1991.
R. Goyal, *Monolithic Microwave Integrated Circuits: Technology and Design*, Norwood, MA: Artech House, 1989.
Y. Konishi, *Microwave Integrated Circuits*, New York: Marcel Dekker, 1991.
P. H. Ladbrooke, *MMIC Design GaAs FETs and HEMTs*, Norwood, MA: Artech House, 1989.
S. Y. Liao, *Microwave Solid-State Devices*, Englewood Cliffs, NJ: Prentice-Hall, 1985.
S. M. Sze, *Semiconductor Devices—Physics and Technology*, New York: Wiley, 1985.
T. G. van de Roer, *Microwave Electronic Devices*, London: Chapman & Hall, 1994.
E. A. Wolff, R. Kaul, *Microwave Engineering and Systems Applications*, New York: Wiley, 1988.

DOMINIQUE SCHREURS
Catholic University of Leuven